

Communication

# 2-Propanol Activation on the Low Index $\text{Co}_3\text{O}_4$ Surfaces: A Comparative Study Using Molecular Dynamics Simulations

Amir Hossein Omranpoor \* and Stephane Kenmoe \*

Department of Theoretical Chemistry, University of Duisburg-Essen, D-45141 Essen, Germany

\* Correspondence: amir.omranpoor@uni-due.de (A.H.O.); stephane.kenmoe@uni-due.de (S.K.)

**Abstract:** We used ab initio molecular dynamics simulations to compare the activation of 2-propanol on the low index  $\text{Co}_3\text{O}_4$  (111), (110) and (001) surfaces in dry conditions. The thermal and surface assisted decomposition of a film of 2-propanol to 2-propoxide on the B-termination of each surface was monitored and analyzed. The investigations suggest an activity order of  $\text{Co}_3\text{O}_4$  (111) > (110) > (001). On all surfaces, the  $\text{Co}^{3+}$  serve as adsorption sites. On the B-terminated (111) surface, full dissociation of all 2-propanol molecules at the interface is observed, accompanied by a Mars-van Krevelen-type mechanism upon pre-hydroxylation of the surface. The active regions show  $\text{Co}^{3+}\text{--O}_2\text{-propoxide}\text{--Co}^{2+}$  bridges where the coordinatively unsaturated  $\text{Co}^{2+}$  ions also participate in the adsorption and decomposition of 2-propanol. On the (110) surface, 2-propanol dissociation is driven by temperature, which activates the two-fold coordinatively unsaturated surface oxygens. The (001) surface on which almost no dissociation occurs is the least active. No formation of acetone is observed in the simulations conditions on all surfaces.

**Keywords:** actives regions; activation; 2-propanol; cobalt oxide; Mars-van Krevelen



**Citation:** Omranpoor, A.H.; Kenmoe, S. 2-Propanol Activation on the Low Index  $\text{Co}_3\text{O}_4$  Surfaces: A Comparative Study Using Molecular Dynamics Simulations. *Catalysts* **2024**, *14*, 25. <https://doi.org/10.3390/catal14010025>

Academic Editors: Jie Yin and Xin Du

Received: 1 December 2023

Revised: 18 December 2023

Accepted: 24 December 2023

Published: 28 December 2023



**Copyright:** © 2023 by the authors. Licensee MDPI, Basel, Switzerland. This article is an open access article distributed under the terms and conditions of the Creative Commons Attribution (CC BY) license (<https://creativecommons.org/licenses/by/4.0/>).

## 1. Introduction

Selective oxidation of primary alcohols plays a crucial role in the environmentally friendly synthesis of organic oxygenated compounds. While gas phase oxidation processes have been studied to a respectable level, the understanding of these processes in the liquid phase, on which relies on most industrial processes, is still under development. Addressing the complexity of liquid phase catalytic processes in operando conditions requires the development of robust and systematic approaches in order to better manipulate the different factors governing the catalysts' efficiency [1,2]. These include the nature of the reaction medium, the structure of the catalysts, oxidant selection, temperature or light.

Transition metal oxides (TMOs) are promising candidates for heterogeneous catalysis due to their abundance, low cost and good catalytic activity. Among the TMOs,  $\text{Co}_3\text{O}_4$  catalysts have demonstrated potential application in energy production and environmentally friendly technological processes. For example, they have shown remarkable performance in methane combustion [3], water oxidation [4], CO oxidation [5], or the selective oxidation of hydrocarbons [6]. Propanol oxidation has recently captured particular attention because of its numerous potential technological applications [7–12] and has triggered studies on the selective oxidation of 2-propanol for the production of acetone on  $\text{Co}_3\text{O}_4$  spinel catalysts as they show beneficial electronic, magnetic and redox properties [13,14].

Anke et al. [15] observed high activity and selectivity on bulk  $\text{Co}_3\text{O}_4$  catalysts during gas phase selective oxidation of 2-propanol. The highest conversion rates of 2-propanol to acetone were observed in between 373 K and 573 K, with a maximum conversion rate close to 100% achieved at 430 K. A similar finding was reported in Ref. [16], where complete conversion and 100% selectivity for 2-propanol oxidation to acetone was observed at 430 K on  $\text{Co}_3\text{O}_4$  nanospheres exposing the (110) surface orientation. In another study [17], the impact of Co concentration on 2-propanol oxidation on  $\text{Co}_{1+x}\text{Fe}_{2-x}\text{O}_4$  spinel oxides was

investigated, both in gas and liquid phases. The study revealed that iron-free  $\text{Co}_3\text{O}_4$  samples have the highest activity as the catalytic activity increased with Co content. Moreover, XPS analysis showed that  $\text{Co}^{3+}$  sites were more active than  $\text{Co}^{2+}$  sites as also found by complementary density functional theory (DFT) calculations performed on the (100) and (110) surfaces [15,16].

For a better understanding of the factors governing the catalytic performance of  $\text{Co}_3\text{O}_4$  spinel nanocatalysts with respect to 2-propanol oxidation to acetone, more theoretical insights need to be provided. We recently used ab initio molecular dynamics (AIMD) simulations to study the role of temperature, surface structure and electrochemical environment on the oxidation process [18]. In a following study, we combined static DFT + U calculations and theoretical XANES to investigate the electronic properties of the active sites during 2-propanol oxidation to acetone on the B-termination of the  $\text{Co}_3\text{O}_4$  (001) surface in dry and humid conditions [19]. Recently, we studied the interaction of 2-propanol with the  $\text{Co}_3\text{O}_4$  (001) surface by vibrational sum frequency spectroscopy and AIMD simulations, both near ambient conditions [20]. This allowed insight at the molecular level, into the pathways of catalytic oxidation. In particular, the multifaceted role of water at the interface for the electrochemical oxidation of 2-propanol in aqueous solution was elucidated to a good extent.

The above-mentioned studies shed light on key catalytic properties such as the local environment of active sites, the binding mechanisms, coordination environment, spin, and oxidation states of active sites, the influence of aqueous solvation and the elemental composition of the surface as well as the vapor pressure of alcohol on the reactivity. However, these studies were restricted to the (001) surfaces. For a complete picture of the interplay between the parameters that governs the catalytic performance of  $\text{Co}_3\text{O}_4$  spinel nanocatalysts, a comprehensive study of the (111) surfaces, highly exposed on naturally grown nanoparticles [21,22] as well as the (110) exposed on nanospheres [16] and found to be reactive to 2-propanol oxidation needs to be performed.

In this study, we use AIMD simulations to investigate the interaction of a film of 2-propanol with the low index  $\text{Co}_3\text{O}_4$  (111) and (110) surfaces. As a first step towards the partial oxidation and formation of acetone, we investigate the activation of 2-propanol and decomposition to 2-propoxide in dry conditions. We monitor the surfaces reactivity towards 2-propanol adsorption at catalytically relevant temperatures and compare it with the previously studied (001) surface. To shed some light on the structure-activity relationship, we analyze the structural response of the surfaces to adsorption and provide fundamental insight into the underlying surface assisted mechanisms that promote 2-propanol activation.

## 2. Computational Details

We considered orthorhombic simulation cells, with  $(2 \times 2)$  periodicity in the lateral directions ( $x, y$ ) corresponding to  $19.81 \text{ \AA} \times 11.44 \text{ \AA}$  and  $22.88 \text{ \AA} \times 16.18 \text{ \AA}$ , in which  $\text{Co}_3\text{O}_4$  (111) and (110) surfaces interact with a film of eight 2-propanol molecules, respectively. The catalytically active B-terminations [23–26] of the surfaces were considered. The respective surfaces were modelled by slabs consisting of 13 and 8 atomic layers and the bottom 5 and 3 layers of the slab were fixed at their bulk positions, respectively. Because of the one-sided adsorption of the film of molecules and the asymmetry of the slab, a dipole correction [27] was introduced in the  $z$ -direction of the slab. A vacuum region of  $30 \text{ \AA}$  was also introduced in the same direction to decouple the system from its periodic images.

Spin-polarized Born-Oppenheimer molecular dynamics simulations were conducted using the CP2K/Quickstep package [28]. The Generalized Gradient Approximation (GGA) within the PBE formulation [29] was used to treat the exchange and correlation effects, plus a U correction of the Hubbard type [30] to accurately describe the Co 3d states. The value of  $U = 2 \text{ eV}$  for both  $\text{Co}^{2+}$  and  $\text{Co}^{3+}$  was used as in previous studies. [31] The Grimme D3 correction [32] was considered to account for dispersion interactions.

Core electrons were described using Goedecker-Teter-Hutter (GTH) pseudopotentials. The O 2s and 2p electrons and Co 3s, 3p, 3d, and 4s electrons were considered as valence

electrons. A mixed representation of plane wave functions with an energy cutoff of 500 Ry and a double- $\zeta$  quality local basis set with a single set of polarization functions (DZVP) were used as basis sets. The same type of pseudopotentials (GTH) and polarization functions (DZVP) are also used for carbon and hydrogen atoms. All simulations were conducted at the  $\Gamma$  point.

NVT conditions were imposed on the simulated systems using a Nosé-Hoover thermostat with a time constant of 1 ps and target temperatures of 300 K and 450 K. A simulation time step of 0.5 fs was used to propagate the atomic positions. Following an equilibration period of at least 1 ps for all systems under study, a production phase of approximately 20 ps was considered to compute and analyze the properties of interest.

### 3. Results and Discussion

#### 3.1. $\text{Co}_3\text{O}_4$ (111) Surface

We performed AIMD simulations of eight 2-propanol molecules interacting with the B-terminated (111) surface of a pristine  $\text{Co}_3\text{O}_4$  at 300 K, for 20 ps of total simulation time. Figure 1 shows snapshots of the initial and final equilibrium trajectories. All eight 2-propanol molecules dissociate on the  $\text{Co}^{3+}$  sites on which they sit all along the simulation. The perspective views in Figure 1 provide a clear evidence of the surface hydroxylation as a result of eight proton transfers to the surface lattice oxygens. No further dehydrogenation of 2-propanol leading to the formation of acetone was observed during the whole simulation period.

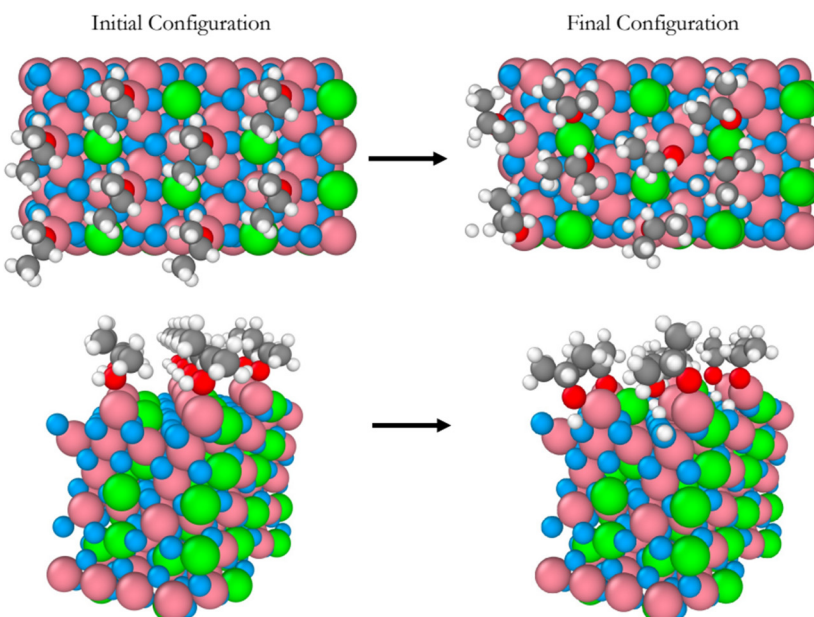


**Figure 1.** Snapshots of the initial and final configurations of the AIMD simulation (top and perspective views) for 2-propanol adsorption on the B-terminated pristine at 300 K.  $\text{Co}_3\text{O}_4$  (111) surface at 300 K.  $\text{Co}^{3+}$  (pink),  $\text{Co}^{2+}$  (green), O in  $\text{Co}_3\text{O}_4$  (blue), O in 2-propanol (red), C (gray), and H (white).

We monitored the changes into the 2-propanol molecules intramolecular bond lengths, O–H, C–H, C–O, and the  $\text{Co}^{3+}$ –O bond length for a dissociatively adsorbed 2-propanol molecule during the 20 ps of simulation as displayed in Figure 2. It is seen that the O–H bond cleavage happens after approximately 2.5 ps of simulation and leads to a shortening of the  $\text{Co}^{3+}$ –O bond length. Additionally, a relatively small shortening of the C–O bond is observed, while the C–H bond remains relatively unchanged throughout the simulation. This supports that no dehydrogenation (C–H bond cleavage) has occurred.

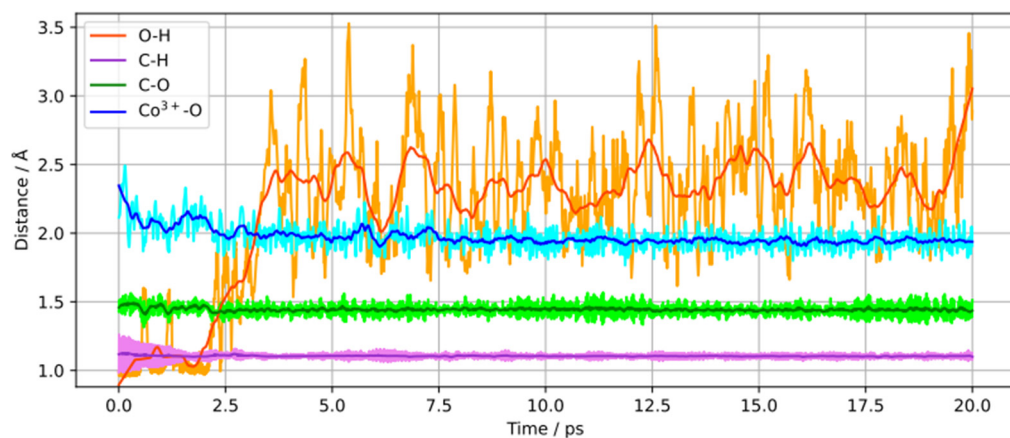


**Figure 2.** Time dependence of O–H, C–H, C–O and  $\text{Co}^{3+}$ –O bond lengths for a dissociatively adsorbed 2-propanol molecule.

The B-terminated (111) surface exposes  $\text{Co}^{3+}$ – $\text{O}_2\text{-propoxide}$ – $\text{Co}^{2+}$  bridges between the adsorption sites and the adsorbates as illustrated by the black lines in Figure 3. The formation of these bridges originates from the unique characteristics of the surface's tetrahedrally coordinated  $\text{Co}^{2+}$  ions. In fact, unlike their counterparts that are coordinatively saturated on the B-terminated (001) surface,<sup>31</sup> these ions are undercoordinated. Their three-fold coordinatively unsaturated nature allows them to participate in 2-propanol adsorption and decomposition.

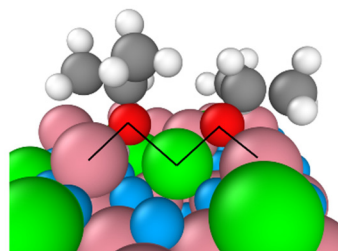


**Figure 3.** Two  $\text{Co}^{3+}$ – $\text{O}_2\text{-propoxide}$ – $\text{Co}^{2+}$  bridges on the B-terminated pristine  $\text{Co}_3\text{O}_4$  (111) surface at 300 K.  $\text{Co}^{3+}$  (pink),  $\text{Co}^{2+}$  (green), O in  $\text{Co}_3\text{O}_4$  (blue), O in 2-propoxide (red), C (gray), and H (white).

On the B-terminated (001) surface, only the topmost layer and, to a lesser extent, the first inner layer were involved in 2-propanol activation [18,19]. In the case of the B-terminated (111) surface, 2-propanol activation is assisted by inner surface layers as illustrated by the charge density difference (CDD) calculated for the final equilibrium trajectory (Figure 4). The  $\text{Co}^{2+}$  ion involved in the  $\text{Co}^{3+}$ – $\text{O}_2\text{-propoxide}$ – $\text{Co}^{2+}$  bridge (Figure 3) and encircled with a dashed black line in Figure 4 contributes significantly to 2-propanol decomposition as it losses electron density upon 2-propanol adsorption. Moreover,  $\text{Co}^{3+}$  ions located in the third inner layer of the slab (orange rectangle), are also electronically involved, as it can be seen by the charge reorganization in the vicinity of these sites.

However, in the adsorbate film, the interaction between the H in  $\text{CH}_3$  groups and the surface oxygens is less pronounced than on the B-terminated (001) surface. No electron density depletion or accumulation is observed in the hydrogens of the  $\text{CH}_3$  groups (black rectangles). This stems from the fact that proton transfer to the surface leads to the hydroxylation of all coordinated, unsaturated surface oxygens (Figure 1), while on the B-terminated (001) surface most of such surface oxygens remain intact. [20]

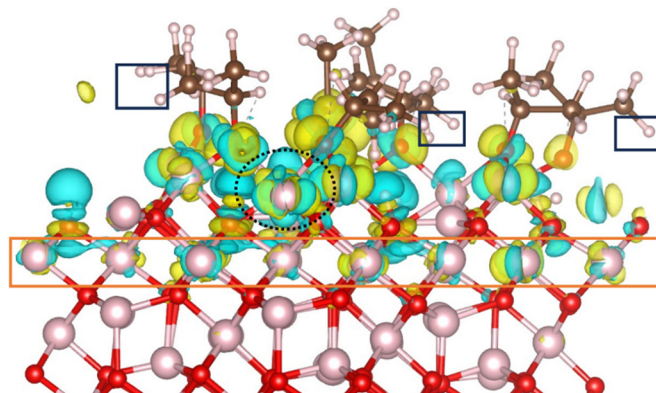


**Figure 4.** Charge density difference plot for the adsorption of 2-propanol on  $\text{Co}^{3+}$  sites of the B-terminated  $\text{Co}_3\text{O}_4$  (111) surface at 300 K. The iso-surfaces are drawn at density levels of  $-0.003$  (cyan) and  $+0.003$  (yellow)  $\text{e Å}^{-3}$ . The yellow regions indicate the accumulation of electron density, while the cyan regions indicate the depletion of electron density.

Interestingly, for a surface pre-exposed to water, with subsequent formation of surface OH groups, a Mars-van Krevelen mechanism happens leading to the formation of water from lattice oxygen. This is illustrated in Figure 5. A lattice OH group receives a hydrogen from 2-propanol, resulting into the formation of a water molecule, 2-propoxide and an oxygen vacancy (black circle).

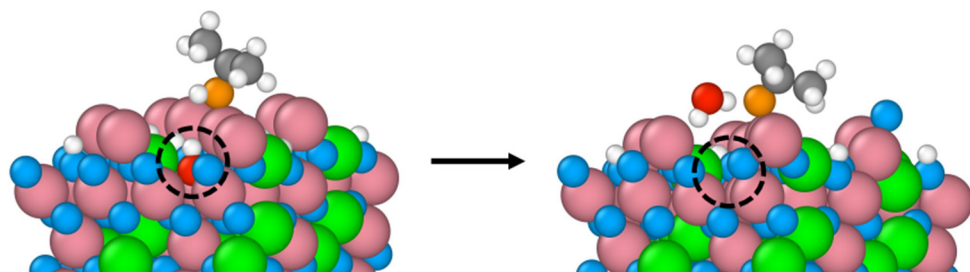


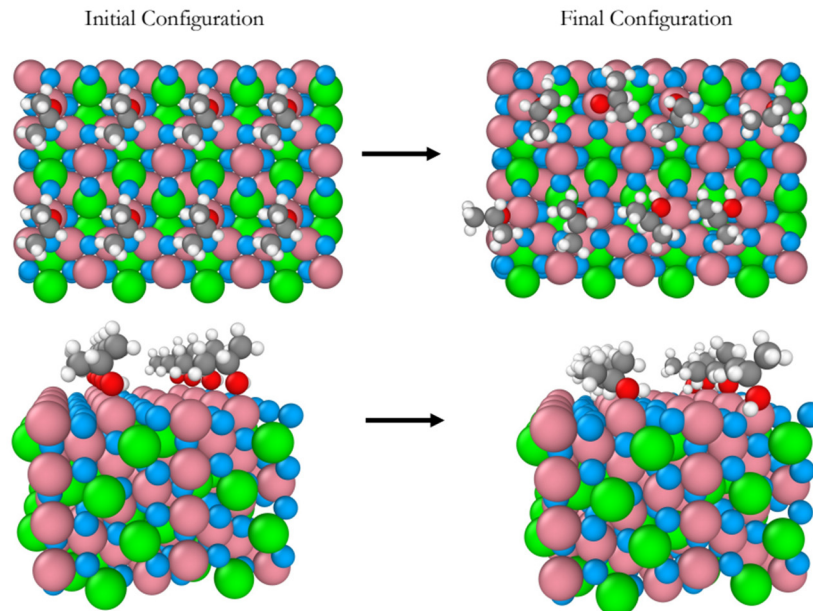
**Figure 5.** Formation of water from surface oxygen through the Mars-van Krevelen mechanism.  $\text{Co}^{3+}$  (pink),  $\text{Co}^{2+}$  (green), O in  $\text{Co}_3\text{O}_4$  (blue), O in 2-propanol (orange), C (gray) and H (white). The lattice oxygen that participates in the Mars-van Krevelen mechanism is denoted in red. The created vacancy is illustrated with a black circle on the right side.

### 3.2. $\text{Co}_3\text{O}_4$ (110) Surface

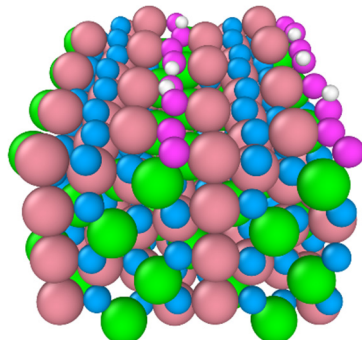
For the B-terminated pristine  $\text{Co}_3\text{O}_4$ (110), the adsorption and decomposition of eight 2-propanol molecules were addressed at 300 K and 450 K during a simulation time of 20 ps. Snapshots of the initial (left) and final (right) of equilibrium trajectories at 300 K are displayed in Figure 6. Six out of the eight 2-propanol molecules adsorb molecularly on top of  $\text{Co}^{3+}$  sites and the two remaining molecules dissociate. The single deprotonation of these two molecules leads to the formation of two 2-propoxide molecules. Like on (001) and (111) surfaces, the  $\text{Co}^{3+}$  adsorption sites remain unchanged throughout the simulation, as it can be seen from the top views in Figure 6. Also, no partial oxidation of 2-propanol and subsequent formation of acetone is observed.

Figure 7 shows the impact of temperature on the reactivity of 2-propanol on the (110) surface. 2-propanol activation increases considerably when the temperature is raised to 450 K. Six 2-propanol molecules dissociate on the surface, resulting in the formation of six surface OH groups. For deeper insights into this temperature driven reactivity, the nature of the lattice oxygen species has been analyzed. They have a lower coordination number and are therefore highly reactive compared to the surface lattice oxygens on the (111) and (001) and A- and B-terminations. The formers are 2-fold coordinated while the latter are either three-fold coordinatively unsaturated or four-fold coordinatively saturated. This

is supported by Figure 7 which shows that all protons are transferred to the “two-fold” coordinatively unsaturated oxygens (in violet). This temperature driven reactivity (110) surface has been also been confirmed experimentally [16].



**Figure 6.** Snapshots of the initial and final configurations of the AIMD simulation (top and perspective views) for 2-propanol adsorption on the B-terminated pristine  $\text{Co}_3\text{O}_4$  (110) surface at 300 K.  $\text{Co}^{3+}$  (pink),  $\text{Co}^{2+}$  (green), O in  $\text{Co}_3\text{O}_4$  (blue), O in 2-propanol (red), C (gray) and H (white).



**Figure 7.** Snapshot of the final configuration of the B-terminated  $\text{Co}_3\text{O}_4$  (110) surface at 450 K. The adsorbed 2-propoxide molecules are removed for visualization. The “two-fold” surface oxygens are denoted in violet.  $\text{Co}^{3+}$  (pink),  $\text{Co}^{2+}$  (green), two-fold O (violet), other O in  $\text{Co}_3\text{O}_4$  (blue), and H (white).

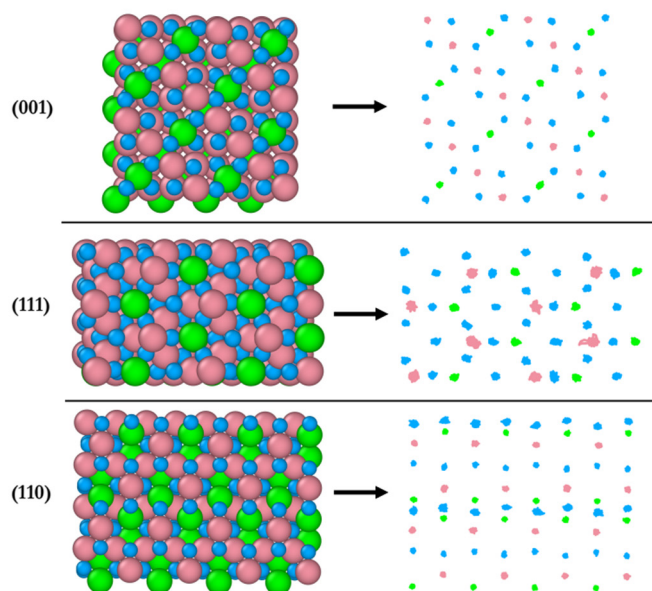
### 3.3. Structure to Activity Relationship

Table 1 summarizes the activity, with respect to 2-propanol conversion to 2-propoxide, of all three surfaces at two different temperatures, 300 K and 450 K. The (111) surface has the highest activity at 300 K or 450 K. The lowest activity is observed on the (001) surface at 450 K where no molecules dissociate [20]. The activity of the (110) surface lies in between that of the (111) and the (001) surfaces, both at 300 K and 450 K. Temperature has the strongest impact on the (110) surface by increasing the activity by an overall 60 percent. No formation of acetone is observed on any of the surfaces.

**Table 1.** Number of initial and final 2-propanol, final 2-propoxide and acetone molecules on the (001), (111), and (110) surfaces at 300 K and 450 K.

	(001)		(110)		(111)	
	300 K	450 K	300 K	450 K	300 K	450 K
Initial 2-propanol	8	8	8	8	8	8
Final 2-propanol	7	8	6	2	0	0
Final 2-propoxide	1	0	2	6	8	8
Final Acetone	0	0	0	0	0	0

Figure 8 shows the structural response of surface atoms during the 20 ps of simulation of the interaction of the B-terminated (001), (111) and (110) surfaces with 2-propanol at 300 K. On the left, the starting surface atom configurations ( $t = 0$ ) are shown, and their trajectories traces are displayed on the right. The (001) surface is found to be the least dynamic compared to the other two surfaces, whereas the (111) surface is the most dynamic as supported by the highest mobility of the  $\text{Co}^{3+}$  ions. This is in line with the pronounced surface relaxations and the formation of  $\text{Co}^{3+}\text{--O}_2\text{-propoxide--Co}^{2+}$  bridges as mentioned above. The most dynamic atoms of the (110) surface are the two-fold unsaturated surface oxygen atoms identified as those activating the 2-propanol dissociation on the surface. The magnitude of relaxation of atoms on this surface lies in between that of the atoms on the (001) and (111) surfaces.



**Figure 8.** Initial configuration (left) of AIMD simulation (top-view) and trajectory traces (right) of surface atoms for (001), (111), and (110) surfaces at 300 K.  $\text{Co}^{3+}$  (pink),  $\text{Co}^{2+}$  (green), O in  $\text{Co}_3\text{O}_4$ , (blue)).

Recently, diffuse reflectance infrared Fourier transform spectroscopy (DRIFTS) [33] was used to obtain the Vibrational Density of States (power spectra) of 2-propanol adsorbed on various transition metal oxides including  $\text{Co}_3\text{O}_4$ . However, some peaks in the spectra could not be ascribed to specific bands. To shed light on this, we calculated the power spectra of adsorbed 2-propanol on B-terminated (001), (111), and (110) surfaces (Figure 9). The main difference between the three spectra is the region between 2800 and  $3100 \text{ cm}^{-1}$ . The peaks around  $3050 \text{ cm}^{-1}$  and  $3100 \text{ cm}^{-1}$  can be assigned to the symmetric and asymmetric stretching modes of  $\text{CH}_3$ , respectively, and the small band at  $2850 \text{ cm}^{-1}$  to the C–H bonds. Additionally, the difference in the  $1100\text{--}1300 \text{ cm}^{-1}$  region can be attributed to the O–H bending mode. There is no C–O bending mode, contributing to the bands around

1700  $\text{cm}^{-1}$  and indicative of acetone formation. Similarly, the O–H stretching mode (peak around 3600–3700  $\text{cm}^{-1}$ ) does not appear, which supports the involvement of the respective H into H-bonding or transfer to the surface.

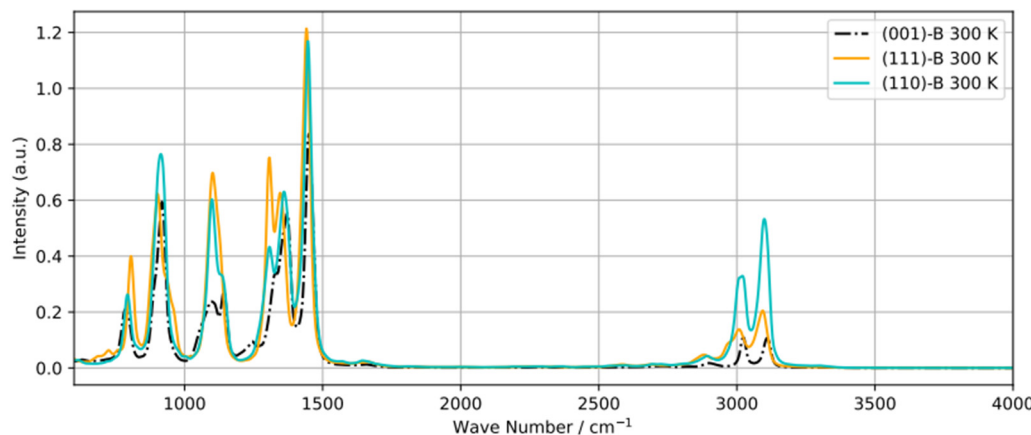


**Figure 9.** Power spectra of an adsorbed 2-propanol molecule equilibrated at 300 K on B-terminated (001), (111) and (110) surfaces.

#### 4. Conclusions

In this work, we used spin-polarized Born-Oppenheimer molecular dynamics simulations to study the interaction of  $\text{Co}_3\text{O}_4$  low index surfaces with a film of 2-propanol molecules, considering the catalytically active B-terminations of the surfaces. Our investigations showed that the (111) surface exhibits higher surface reactivity towards 2-propanol activation compared to the (110) and (001) surfaces. Complete dissociation of 2-propanol to 2-propoxide is observed on the (111) surface at 300 K and 450 K. The  $\text{Co}^{3+}$  ions are the adsorption sites. However, the neighboring coordinatively unsaturated three-fold  $\text{Co}^{2+}$  also participate in the reaction via the formation of  $\text{Co}^{3+}\text{--O}_2\text{-propoxide}\text{--Co}^{2+}$  bridges. Upon hydroxylation of the surface at room temperature, 2-propanol activation is accompanied by a Mars-van Krevelen mechanism which yields the formation of 2-propoxide and molecular water. On the (110) surface, the temperature activates the surface two-fold coordinatively unsaturated oxygens as illustrated by the improvement in the activity by 60% when the temperature is increased to 450 K. The (001) surface studied in previous works is the least active, and the activity order of magnitude reads (111) > (110) > (001). Our findings are a primordial step towards the understanding of the complex face-dependent activity of  $\text{Co}_3\text{O}_4$ , nanocatalysts [34–36] vis-à-vis to the liquid phase 2-propanol oxidation to acetone. Namely, the role of the surface elemental composition and temperature have been elucidated in the absence of a solvent. The study may also indicate the possible key role of the electrochemical nature of the reaction medium at the interface for the partial oxidation of 2-propanol to acetone as demonstrated previously for a single 2-propanol molecule diluted in an aqueous film on the (001) surface [18]. Ongoing studies being performed in our group are addressing the impact of aqueous solvation on the oxidation process at various oxidative conditions, for the three surfaces in interaction with a film of 2-propanol molecules.

**Author Contributions:** Conceptualization, A.H.O. and S.K.; methodology, A.H.O. and S.K.; validation, A.H.O.; formal analysis, A.H.O.; investigation, A.H.O. and S.K.; resources, A.H.O. and S.K.; data curation, A.H.O. and S.K.; writing—original draft preparation, A.H.O.; writing—review and editing, S.K.; visualization, A.H.O. and S.K.; supervision, S.K.; project administration, S.K.; funding acquisition, A.H.O. and S.K. All authors have read and agreed to the published version of the manuscript.

**Funding:** This research was funded by the Deutsche Forschungsgemeinschaft (DFG, German Research Foundation)—388390466—TRR 247 within the work of Project A6.

**Data Availability Statement:** The data that support the findings of this study are available from the corresponding authors upon reasonable request.

**Acknowledgments:** The authors acknowledge the computing time granted by the Center for Computational Sciences and Simulation (CCSS) of the University of Duisburg-Essen and provided on the supercomputer magnitUDE (DFG grants INST 20876/209-1 FUGG, INST 20876/243-1 FUGG) at the Zentrum für Informations-und Mediendienste (ZIM). A.H.O. is thankful to the International Max Planck Research School for Interface Controlled Materials for Energy Conversion (IMPRS-SurMat) for a Ph.D. Fellowship.

**Conflicts of Interest:** The authors declare no conflict of interest.

## References

1. Najafshirtari, S.; Ortega, K.F.; Douthwaite, M.; Pattisson, S.; Hutchings, G.J.; Bondue, C.J.; Tschulik, K.; Waffel, D.; Peng, B.; Deitermann, M.; et al. A perspective on heterogeneous catalysts for the selective oxidation of alcohols. *Chem. Eur. J.* **2021**, *27*, 16809–16833. [[CrossRef](#)]
2. Grasselli, R.K. Fundamental principles of selective heterogeneous oxidation catalysis. *Top. Catal.* **2002**, *21*, 79–88. [[CrossRef](#)]
3. Hu, L.; Peng, Q.; Li, Y. Selective synthesis of  $\text{Co}_3\text{O}_4$  nanocrystal with different shape and crystal plane effect on catalytic property for methane combustion. *J. Am. Chem. Soc.* **2008**, *130*, 16136–16137. [[CrossRef](#)]
4. Jiao, F.; Frei, H. Nanostructured cobalt oxide clusters in mesoporous silica as efficient oxygen-evolving catalysts. *Angew. Chem.* **2009**, *121*, 1873–1876. [[CrossRef](#)]
5. Xie, X.; Li, Y.; Liu, Z.-Q.; Haruta, M.; Shen, W. Low-temperature oxidation of CO catalysed by  $\text{Co}_3\text{O}_4$  nanorods. *Nature* **2009**, *458*, 746–749. [[CrossRef](#)]
6. Waidhas, F.; Haschke, S.; Khanipour, P.; Fromm, L.; Görling, A.; Bachmann, J.; Katsounaros, I.; Mayrhofer, K.J.; Brummel, O.; Libuda, J. Secondary alcohols as rechargeable electrofuels: Electrooxidation of isopropyl alcohol at pt electrodes. *ACS Catal.* **2020**, *10*, 6831–6842. [[CrossRef](#)]
7. Doheim, M.M.; El-Shobaky, H.G. Catalytic conversion of ethanol and iso-propanol over  $\text{ZnO}$ -treated  $\text{CoO}/\text{AlO}$  solids. *Colloids Surf. A* **2002**, *204*, 169–174. [[CrossRef](#)]
8. Yang, T.; Kastenmeier, M.; Ronovský, M.; Fusek, L.; Skála, T.; Waidhas, F.; Bertram, M.; Tsud, N.; Matvija, P.; Prince, K.C.; et al. Selective electrooxidation of 2-propanol on Pt nanoparticles supported on CoO: An in-situ study on atomically defined model systems. *J. Phys. D* **2021**, *54*, 164002. [[CrossRef](#)]
9. Markiewicz, M.E.P.; Bergens, S.H. A liquid electrolyte alkaline direct 2-propanol fuel cell. *J. Power Sources* **2010**, *195*, 7196–7201. [[CrossRef](#)]
10. Santasalo, A.; Vidal-Iglesias, F.J.; Solla-Gullón, J. Electrooxidation of methanol and 2-propanol mixtures at platinum single crystal electrodes. *Electrochim. Acta* **2009**, *54*, 6576–6583. [[CrossRef](#)]
11. Otomo, J.; Li, X.; Kobayashi, T.; Wen, C.J.; Nagamoto, H.; Takahashi, H. AC-impedance spectroscopy of anodic reactions with adsorbed intermediates: Electro-oxidations of 2-propanol and methanol on carbon-supported Pt catalyst. *J. Electroanal. Chem.* **2004**, *573*, 99–109.
12. Pastor, E.; González, S.; Arvia, A.J. Electrocatalysis of isopropanol on platinum in acids studied by DEMS and FTIRS. *J. Electroanal. Chem.* **1995**, *395*, 233–242. [[CrossRef](#)]
13. Chen, J.; Wu, X.; Selloni, A. Electronic structure and bonding properties of cobalt oxide in the spinel structure. *Phys. Rev. B* **2011**, *83*, 245204. [[CrossRef](#)]
14. Kenmoe, S.; Douma, D.H.; Raji, A.T.; M'Passi-Mabiala, B.; Gotsch, T.; Girgsdies, F.; Knop-Gericke, A.; Schlogl, R.; Spohr, E. X-ray absorption near-edge structure (xanes) at the o k-edge of bulk  $\text{Co}_3\text{O}_4$ : Experimental and theoretical studies. *Nanomaterials* **2022**, *12*, 921. [[CrossRef](#)]
15. Anke, S.; Bendt, G.; Sinev, I.; Hajiyani, H.; Antoni, H.; Zegkinoglou, I.; Jeon, H.; Pentcheva, R.; Roldan Cuenya, B.; Schulz, S.; et al. Selective 2-propanol oxidation over unsupported  $\text{Co}_3\text{O}_4$  spinel nanoparticles: Mechanistic insights into aerobic oxidation of alcohols. *ACS Catal.* **2019**, *9*, 5974–5985. [[CrossRef](#)]
16. Falk, T.; Anke, S.; Hajiyani, H.; Saddeler, S.; Schulz, S.; Pentcheva, R.; Peng, B.; Muhler, M. Influence of the particle size on selective 2-propanol gas-phase oxidation over  $\text{Co}_3\text{O}_4$  nanospheres. *Catal. Sci. Technol.* **2021**, *11*, 7552–7562. [[CrossRef](#)]
17. Falk, T.; Budiyanto, E.; Dreyer, M.; Pflieger, C.; Waffel, D.; Büker, J.; Weidenthaler, C.; Ortega, K.F.; Behrens, M.; Tüysüz, H.; et al. Identification of active sites in the catalytic oxidation of 2-propanol over  $\text{Co}_{1+x}\text{Fe}_{2-x}\text{O}_4$  spinel oxides at solid/liquid and solid/gas interfaces. *ChemCatChem* **2021**, *13*, 2942–2951. [[CrossRef](#)]
18. Omranpoor, A.; Kox, T.; Spohr, E.; Kenmoe, S. Influence of temperature, surface composition and electrochemical environment on 2-propanol decomposition at the  $\text{Co}_3\text{O}_4$  (001)/ $\text{H}_2\text{O}$  interface. *Appl. Surf. Sci. Adv.* **2022**, *12*, 100319. [[CrossRef](#)]
19. Douma, D.H.; Nono, K.N.; Omranpoor, A.H.; Lamperti, A.; Debernardi, A.; Kenmoe, S. Probing the local environment of active sites during 2-propanol oxidation to acetone on the  $\text{Co}_3\text{O}_4$  (001) surface: Insights from first principles O K-edge XANES spectroscopy. *J. Phys. Chem. C* **2023**, *127*, 5351–5357. [[CrossRef](#)]

20. Omranpoor, A.H.; Bera, A.; Bullert, D.; Linke, M.; Salamon, S.; Webers, S.; Wende, H.; Hasselbrink, E.; Spohr, E.; Kenmoe, S. 2-Propanol interacting with  $\text{Co}_3\text{O}_4$  (001): A combined vSFS and AIMD study. *J. Chem. Phys.* **2023**, *158*, 164703. [CrossRef] [PubMed]
21. Zasada, F.; Piskorz, W.; Cristol, S.; Paul, J.-F.; Kotarba, A.; Sojka, Z. Periodic density functional theory and atomistic thermodynamic studies of cobalt spinel nanocrystals in wet environment: Molecular interpretation of water adsorption equilibria. *J. Phys. Chem. C* **2010**, *114*, 22245–22253. [CrossRef]
22. Zasada, F.; Piskorz, W.; Stelmachowski, P.; Kotarba, A.; Paul, J.-F.; Płociński, T.; Kurzydłowski, K.J.; Sojka, Z. Periodic DFT and HR-STEM studies of surface structure and morphology of cobalt spinel nanocrystals. retrieving 3D shapes from 2D images. *J. Phys. Chem. C* **2011**, *115*, 6423–6432. [CrossRef]
23. Montoya, A.; Haynes, B.S. Periodic density functional study of  $\text{Co}_3\text{O}_4$  surfaces. *Chem. Phys. Lett.* **2011**, *502*, 63–68. [CrossRef]
24. Yan, G.; Sautet, P. Surface Structure of  $\text{Co}_3\text{O}_4$  (111) under Reactive Gas-Phase Environments. *ACS Catal.* **2019**, *9*, 6380–6392. [CrossRef]
25. Selcuk, S.; Selloni, A. DFT+U Study of the Surface Structure and Stability of  $\text{Co}_3\text{O}_4$ (110): Dependence on U. *J. Phys. Chem. C* **2015**, *119*, 9973–9979. [CrossRef]
26. Creazzo, F.; Ruth Galimberti, D.; Pezzotti, S.; Gaigeot, M.-P. DFT-MD of the (110)- $\text{Co}_3\text{O}_4$  cobalt oxide semiconductor in contact with liquid water, preliminary chemical and physical insights into the electrochemical environment. *J. Chem. Phys.* **2019**, *150*, 041721. [CrossRef] [PubMed]
27. Neugebauer, J.; Scheffler, M. Adsorbate-substrate and adsorbate-adsorbate interactions of Na and K adlayers on Al (111). *Phys. Rev. B* **1992**, *46*, 16067. [CrossRef]
28. CP2K Is Freely. 2016. Available online: <http://www.cp2k.org/> (accessed on 11 June 2018).
29. Perdew, J.P.; Burke, K.; Ernzerhof, M. Generalized Gradient Approximation Made Simple. *Phys. Rev. Lett.* **1996**, *77*, 3865–3868. [CrossRef]
30. Hubbard, J.; Flowers, B.H. Electron correlations in narrow energy bands. *Proc. R. Soc. Lond. Ser. A Math. Phys. Sci.* **1963**, *276*, 238–257.
31. Kox, T.; Spohr, E.; Kenmoe, S. Impact of solvation on the structure and reactivity of the  $\text{Co}_3\text{O}_4$  (001)/ $\text{H}_2\text{O}$  interface: Insights from molecular dynamics simulations. *Front. Energy Res.* **2020**, *8*, 312. [CrossRef]
32. Grimme, S.; Antony, J.; Ehrlich, S.; Krieg, H. A consistent and accurate ab initio parametrization of density functional dispersion correction (DFT-D) for the 94 elements H-Pu. *J. Chem. Phys.* **2010**, *132*, 154104. [CrossRef] [PubMed]
33. Dreyer, M.; Cruz, D.; Hagemann, U.; Zeller, P.; Heidelmann, M.; Salamon, S.; Landers, J.; Rabe, A.; Ortega, K.F.; Najafishirtari, S.; et al. The effect of water on the 2-propanol oxidation activity of Co-substituted  $\text{LaFe}_{1-x}\text{Co}_x\text{O}_3$  perovskites. *Chem. Eur. J.* **2021**, *27*, 17127–17144. [CrossRef] [PubMed]
34. Gao, R.; Zhu, J.; Xiao, X.; Hu, Z.; Liu, J.; Liu, X. Facet-Dependent Electrocatalytic Performance of  $\text{Co}_3\text{O}_4$  for Rechargeable Li-O<sub>2</sub> Battery. *J. Phys. Chem. C* **2015**, *119*, 4516–4523. [CrossRef]
35. Liu, Z.; Amin, H.M.A.; Peng, Y.; Corva, M.; Pentcheva, R.; Tschulik, K. Facet-Dependent Intrinsic Activity of Single  $\text{Co}_3\text{O}_4$  Nanoparticles for Oxygen Evolution Reaction. *Adv. Funct. Mater.* **2023**, *33*, 2210945. [CrossRef]
36. Zhang, Z.; Yang, Z.; Wei, C.; Liu, Z.; Mu, T. Facet-dependent electrocatalytic oxidation activity of  $\text{Co}_3\text{O}_4$  nanocrystals for 5-hydroxymethylfurfural. *Green Chem.* **2023**, *25*, 8196–8206. [CrossRef]

**Disclaimer/Publisher’s Note:** The statements, opinions and data contained in all publications are solely those of the individual author(s) and contributor(s) and not of MDPI and/or the editor(s). MDPI and/or the editor(s) disclaim responsibility for any injury to people or property resulting from any ideas, methods, instructions or products referred to in the content.

# DuEPublico

Duisburg-Essen Publications online

UNIVERSITÄT  
DUISBURG  
ESSEN

*Offen im Denken*

**ub** | universitäts  
bibliothek

This text is made available via DuEPublico, the institutional repository of the University of Duisburg-Essen. This version may eventually differ from another version distributed by a commercial publisher.

**DOI:** 10.3390/catal14010025

**URN:** urn:nbn:de:hbz:465-20240806-144159-8



This work may be used under a Creative Commons Attribution 4.0 License (CC BY 4.0).